

QED Test at LEP200 Energies in the Reaction $e^+e^- \rightarrow \gamma\gamma(\gamma)$

Angela Bajo^o, Irina Dymnikova^{*}, Alexander Sakharov[†],
 Eusebio Sanchez^o, Jürgen Ulbricht[†] and Jiawei Zhao[‡]

[†]*Labor für Höchenergiephysik, ETH-Hönggerberg, HPK-Gebäude, CH-8093 Zürich, Switzerland*

[‡]*Chinese University of Science and Technology, USTC, Anhui 230029 Hefei, P.R.China*

^o*Centro de Investigaciones Energeticas, Medioambientales y Tecnologicas, Avda. Complutense 22, 28040 Madrid, Spain*

^{*}*Institute of Mathematics and Informatics, University of Warmia and Mazury, PL-10-561 Olsztyn, Poland*

Abstract. The measurements of the QED reaction $e^+e^- \rightarrow \gamma\gamma(\gamma)$ performed with the L3 detector are used to search for new physics phenomena beyond the Standard Model. No evidence for these phenomena is found and new limits on their parameters are set. First the reaction is used to constrain a model of an excited electron and second to study contact interactions. The total and differential cross sections for the process $e^+e^- \rightarrow \gamma\gamma(\gamma)$, are measured at energies from 91 GeV to 202 GeV using the data collected with the L3 detector from 1991 to 1999. The L3 data set lower limits on the mass of an excited electron $m_{e^*} > 402$ GeV, on the QED cutoff parameters $\Lambda_+ > 415$ GeV, $\Lambda_- > 258$ GeV and on the contact interaction energy scale $\Lambda > 1687$ GeV. The last parameter limits the size of the interaction area to $R < 1.17 \times 10^{-17}$ cm. Some limits on the string and quantum gravity scales are also discussed.

INTRODUCTION

This paper describes a study of the process $e^+e^- \rightarrow \gamma\gamma(\gamma)$ using data recorded with the L3 detector at LEP at center-of-mass energies (CM) from 91 GeV to 202 GeV. These processes are dominated by QED even at high LEP energies. Since the differential cross-section is well known from QED [1], any deviation from this expectation hints at non-standard physics processes contributing to the photonic final states. Any non-QED effects within the general framework of effective Lagrangian theory are expected to increase with CM [2]. A comparison of the measured photon angular distribution with the QED expectation has been used to put limits on the QED cut-off parameters [3], and non-standard γe^+e^- and $\gamma\gamma e^+e^-$ couplings [2]. The obtained limit on the QED cut-off parameters put constraints on the size of the interaction area, which can be connected to the size of selfgravitating particlelike structure with de Sitter vacuum core [4]. The other application

of our results is strongly related to the study of low energy effects of large extra dimensions [5] in the string theory framework [6,7].

We report on the measurements of total and differential cross section of the $e^+e^- \rightarrow \gamma\gamma(\gamma)$ reaction between 1991 and 1999. Previous results have been published by the L3 at lower CM energies [8] and by the other groups [9].

THE L3 DETECTOR AND EVENT SELECTION

The L3 detector Fig.1 is described in details in [10]. The individual components of the detector are the vertex silicon microstrip detector (SMD), the central tracking chamber (TEC) working in a time expansion mode, the electromagnetic calorimeter composed on bismuth germanium oxide crystals (BGO) with a barrel region ($42^\circ < \theta < 138^\circ$) and two end-caps ($11^\circ < \theta < 37^\circ$ and $143^\circ < \theta < 169^\circ$), a layer of scintillation counters used for time measurements, an uranium hadronic calorimeter, and a high precision muon spectrometer. All sub-detectors are located in a 12m diameter magnet which provides a uniform field of 0.5 T parallel to the beam direction. Forward BGO calorimeter on either side of the detector measure the luminosity by detecting small-angle Bhabha events. Electrons and photons are measured in the electromagnetic calorimeter with an energy resolution better than 2% for particle energies above 1GeV. Fitting a shower shape to the signals of the individual crystals of the electromagnetic bump results in a spatial resolution of about 2 mm in front of the calorimeter [11]. The discrimination of electrons and photons depends on the track information of the central tracking chamber. This chamber is divided into 24 outer sectors with 54 anode wires and 12 inner sectors with 8 anode wires. It detects charged particles reliably in the polar angle range

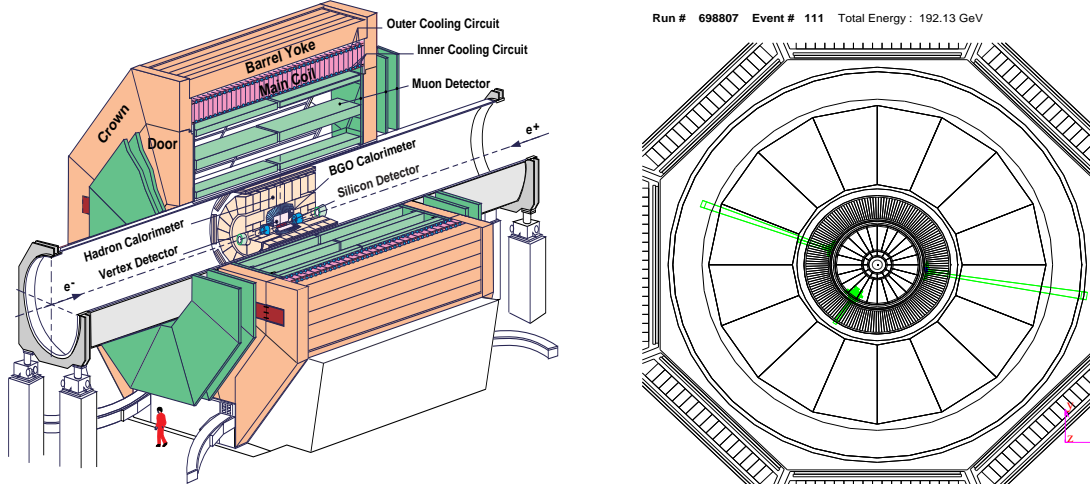


FIGURE 1. The L3 detector (left side) and a typical $e^+e^- \rightarrow \gamma\gamma(\gamma)$ event. The columns show the energy deposit in the BGO crystals.

TABLE 1. The luminosity, selection efficiencies at the different CM's, the number of observed events and the total cross section.

| Energy (GeV) | Luminosity (pb ⁻¹) | Efficiency (%) | Event number | $\sigma_{e^+e^-\rightarrow\gamma\gamma(\gamma)}^{tot}$ (pb) |
|--------------|--------------------------------|----------------|--------------|---|
| 192 | 29 | 61 | 154 | $8.74 \pm 0.71 \pm 0.17$ |
| 196 | 82 | 61 | 427 | $8.51 \pm 0.41 \pm 0.16$ |
| 200 | 76 | 62 | 425 | $9.13 \pm 0.44 \pm 0.17$ |
| 202 | 37 | 62 | 163 | $7.15 \pm 0.56 \pm 0.14$ |

of $18^\circ < \theta < 162^\circ$. The measurement of the (r, ϕ) coordinates is performed with a single wire resolution of about 50 μm .

For the event selection an ideal event of type $e^+e^- \rightarrow \gamma\gamma(\gamma)$ has a characteristic signature in the detector. Almost all of its energy is deposited in the electromagnetic calorimeter (BGO) and there is no track in the TEC Fig. 1.

To select an event there must be at least two photon candidates with polar angles θ_γ (angle with respect to the beam) between 20° and 160° with an angular separation of more than 60° between two most energetic photons, and no other activity in the detector.

A shower in the electromagnetic calorimeter must show a profile consistent with that of a photon and an energy above 2 GeV. To reject $e^+e^- \rightarrow \nu\bar{\nu}\gamma\gamma$ and cosmic rays, we require that the sum of the energies of the photon candidates be larger than $\sqrt{s}/2$. The remaining backgrounds are $e^+e^- \rightarrow e^+e^-(\gamma\gamma)$ and $e^+e^- \rightarrow \tau^+\tau^-(\gamma\gamma)$ with charged particles in the beam pipe. These contributions are estimated from Monte Carlo (MC) simulations using BHWIDE for Bhabha events and KORALZ for τ events, and are found to be negligible. The acceptance is computed applying the same analysis to a sample of $e^+e^- \rightarrow \gamma\gamma(\gamma)$ events generated using an order α^3 MC generator [1,8] passed through the L3 simulation (see refs. in [8]) and reconstruction programs. As an example, the selection efficiencies to detect at least two photons inside the fiducial volume are represented in Table 1 for four energies. The efficiency of the calorimetric energy trigger is estimated to be above 99.7 % .

ANALIZES OF $e^+e^- \rightarrow \gamma\gamma(\gamma)$ EVENTS

Applying this selection cuts the number of observed events, classified according to the number of isolated photons within the range $20^\circ < \theta_\gamma < 160^\circ$, as presented in Table 1 at the four different CM energies. No events with 5 or more photons have been observed.

To check the consistency of data and MC, the photons in the events are sorted with respect to their energy $E_{\gamma 1} > E_{\gamma 2} > E_{\gamma 3}$ and compared to MC. This is shown in Fig. 2 together with the distribution of the collinearity angle of first two photons, normalized to 200 GeV. Data and MC are in good agreement for all energies.

The knowledge of the number of events, luminosity and efficiencies allows us to calculate the differential cross section, which is shown in Fig.3 (left side) and

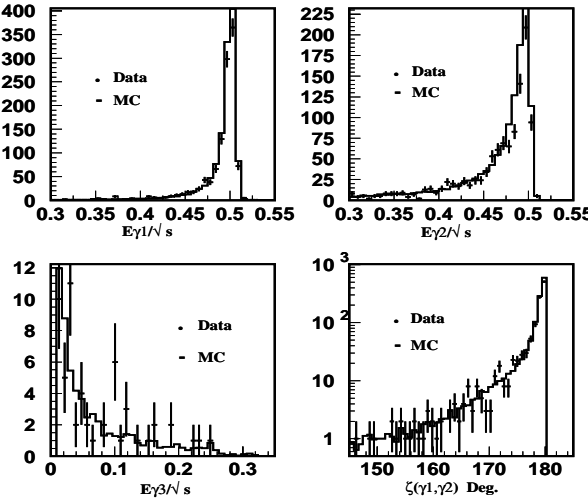


FIGURE 2. The photon energy $E_{\gamma i}$ ($i = 1, 2, 3$) and the collinearity angle distributions are compared with the MC expectation.

normalized to the Born level (right side). The polar angle Θ of event is defined as $\cos \Theta = \frac{1}{2}(|\cos \theta_1| + |\cos \theta_2|)$, where θ_1 and θ_2 are the polar angles of the two most energetic photons in the event. Radiative corrections are quantified in Fig. 3 (right side) as the difference between the differential cross section up to $\mathcal{O}(\alpha^3)$ (solid line) and the Born level (broken line). Excellent agreement between the data and QED predictions is observed up to $\mathcal{O}(\alpha^3)$.

The observed number of events in the fiducial region $20^\circ < \theta < 160^\circ$ corresponds to the total cross sections, which are presented in Table. 1. The first error is statistical and the second one is systematic. The statistical error dominates in the measurement of the cross section at every energy. It has been evaluated by varying the selection cuts and taking into account the finite MC statistic.

A second independent data analysis, with similar cuts, from 90GeV to 202GeV was performed measuring the differential and total cross section of the $e^+e^- \rightarrow \gamma\gamma(\gamma)$ reaction. Both analysis are agreed. Fig.4 shows the total cross section of this analysis compared to the QED predictions up to $\mathcal{O}(\alpha^3)$ level.

LIMITS ON DEVIATIONS FROM QED

In the case of electromagnetic interaction the process $e^+e^- \rightarrow \gamma\gamma(\gamma)$ is ideal to test the QED because it is not interfered by the Z^0 decay. This reaction proceeds via the exchange of a virtual electron in the t – and u – channels, while the s – channel is forbidden due to the angular momentum conservation.

The differential cross section for the process $e^+e^- \rightarrow \gamma\gamma$ in the relativistic limit of lower order QED is given by [12]:

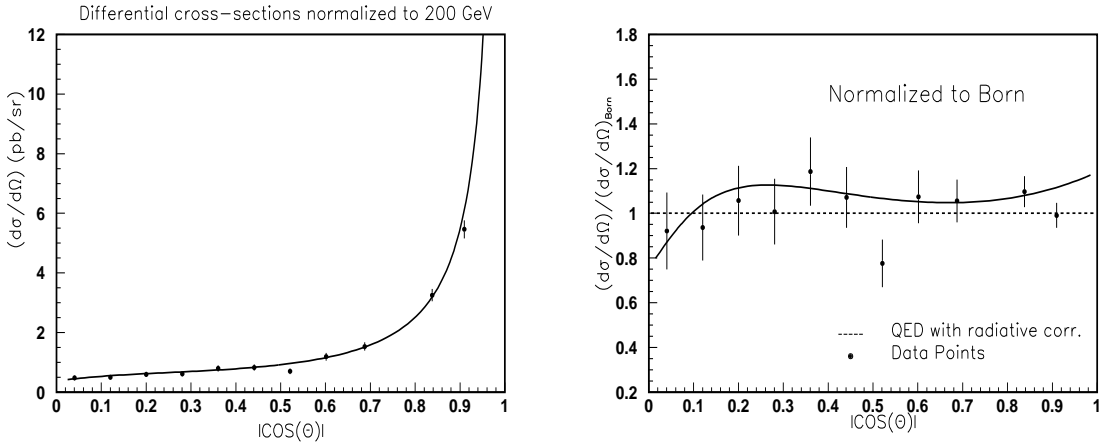


FIGURE 3. The measured angular distribution for the process $e^+e^- \rightarrow \gamma\gamma(\gamma)$ normalized to 200GeV. The points show the experimental data. The solid curve on the left side corresponds to the QED $\mathcal{O}(\alpha^3)$ prediction. The ratio $(d\sigma/d\Omega)/(d\sigma/d\Omega)_{Born}$ is displayed on the right side.

$$\left(\frac{d\sigma}{d\Omega}\right)_{Born} = \frac{\alpha^2}{s} \cdot \frac{1 + \cos^2 \theta}{1 - \cos^2 \theta} \quad (1)$$

where α is the electromagnetic coupling constant and θ is the polar angle of one of the photons. Since two photons can not be distinguished the event angle is defined as positive. A possible deviation from the QED cross section for Bhabha and Möller

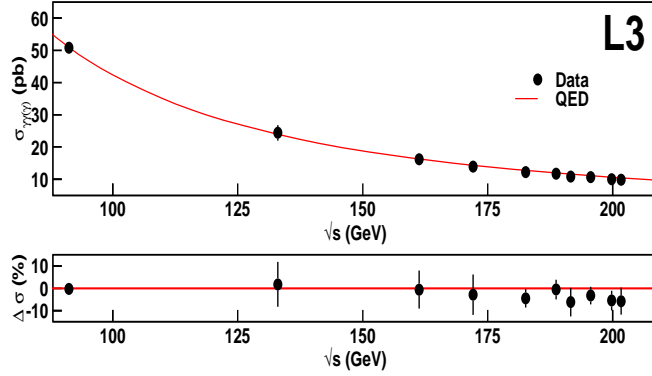


FIGURE 4. Total measured cross-section (points) compared with QED prediction up to $\mathcal{O}(\alpha^3)$ and $\Delta\sigma(\%)$ as a function of CM energy.

scattering are parameterized in terms of cutoff parameters Λ . Such parameters correspond to a short range exponential term added to the Coulomb potential. This ansatz together with $\mathcal{O}(\alpha^3)$ radiative corrections leads to a modification of the photon angular distribution (1)

$$\left(\frac{d\sigma}{d\Omega}\right)_{QED+DEV} = \left(\frac{d\sigma}{d\Omega}\right)_{O(\alpha^3)} (1 + \delta_{DEV}), \quad (2)$$

In the present paper we use the agreement between the data and the QED predictions to constrain the model of an excited electron of mass m_{e^*} which replaces the virtual electron in the QED process [3], as well as to constrain the model with deviation from QED arising from an effective interaction with non-standard $e^+e^-\gamma$ couplings and $e^+e^-\gamma\gamma$ contact terms [2].

The heavy excited electron couples to an electron and a photon via magnetic interaction with an effective gauge invariant Lagrangian of [3].

$$\mathcal{L}_{\text{excited}} = \frac{e\lambda}{2m_{e^*}} \overline{\psi}_{e^*} \sigma_{\mu\nu} \psi_e F^{\mu\nu} \quad (3)$$

In this equation λ is the coupling constant, $F^{\mu\nu}$ the strength electromagnetic field tensor, ψ_{e^*} and ψ_e are the wave functions of the heavy electron and the ordinary electron respectively.

In the case of effective contact interaction with non-standard coupling a cut-off parameter Λ is introduced to describe the scale of the interaction with the following Lagrangian [2]

$$\mathcal{L}_{\text{contact}} = i\overline{\psi}_e \gamma_\mu (D_\nu \psi_e) \left(\frac{\sqrt{4\pi}}{\Lambda_6^2} F^{\mu\nu} + \frac{\sqrt{4\pi}}{\tilde{\Lambda}_6^2} \tilde{F}^{\mu\nu} \right) \quad (4)$$

The effective Lagrangian chosen in this case has an operator of dimension 6, the wave function of the electron is ψ_e , the QED covariant derivative is D_ν , the tilde on $\tilde{\Lambda}_6$ and $\tilde{F}^{\mu\nu}$ stands for dual.

In the case of the excited electron, if the CM energy \sqrt{s} satisfies the condition $s/m_{e^*}^2 \ll 1$, then δ_{DEV} reads

$$\delta_{DEV} = \pm s^2 / 2(1/\Lambda_\pm^4)(1 - \cos^2 \theta) \quad (5)$$

In this approximation, the parameters Λ_\pm are the QED cut-off parameters with $\Lambda_+^2 = m_{e^*}^2/\lambda$. In the case of an arbitrary value of \sqrt{s} the full equation of ref. [3] is used to calculate $\delta_{DEV} = f(m_{e^*})$. In the case of contact interaction δ_{DEV} reads as

$$\delta_{DEV} = s^2 / (2\alpha)(1/\Lambda_6^4 + 1/\tilde{\Lambda}_6^4)(1 - \cos^2 \theta) \quad (6)$$

At the CM under consideration, the χ^2 fit gives for the excited electron $m_{e^*} > 343$ GeV with the QED cut-off parameters $\Lambda_+ > 362$ GeV and $\Lambda_- > 250$ GeV and for non-point like coupling $\Lambda > 1472$ GeV at 95% CL (we set $\Lambda_6 = \tilde{\Lambda}_6 = \Lambda$).

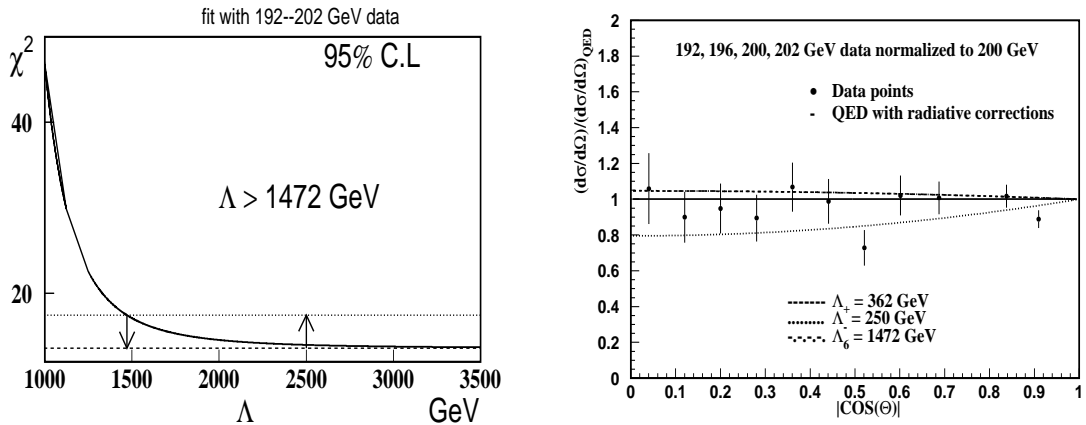


FIGURE 5. The behavior of χ^2 as a function from Λ . The comparison of the measured differential cross section with the QED predictions including the deviations of the parameters Λ_{\pm} and Λ_6 as a function of $|\cos \Theta|$. The cross section is normalized to the radiatively $\mathcal{O}(\alpha^3)$ corrected QED cross section (right side).

The χ^2 as a function of Λ is shown in Fig. 5 (left side) together with differential cross section normalized to the QED one at the $\mathcal{O}(\alpha^3)$ level (right side). The most stringent limit we get from a global χ^2 fit from the results at the CM's 91.2GeV, 133GeV, 161GeV, 172GeV, 183GeV, 189GeV and 200GeV. These limits read $m_{e^*} > 402$ GeV, $\Lambda_+ > 415$ GeV, $\Lambda_- > 258$ GeV and $\Lambda > 1687$ GeV at 95% CL. These scales allow to estimate the upper limits on the characteristic size of the interaction region related to the interactions (4) and (3) respectively. The limit on the contact interaction establishes the characteristic limit of the QED size interaction region to $R \sim \hbar/(m_{e^*}c) < 1.17 \times 10^{-17}$ cm. The behavior of χ^2 as a function of Λ shows no minimum indicating that the size of the interaction region must be smaller than R . We conclude that the most stringent upper limit on scale of the non-point like behavior of electron comes from the contact interaction term.

We found also that all experimental limits on sizes of fundamental particles are smaller than their Compton wavelengths. This fact has been applied to estimate the lower limits on particle sizes in the model of a fundamental particle as a self-gravitating structure with de Sitter vacuum core [4].

Our results could also be applied to study TeV scale quantum gravity [5]. It is possible to suggest that the fundamental scale of gravitational interaction M is as low as TeV [5], whereas the observed weakness of the Newtonian coupling constant $G_N \sim M_{Pl}^{-2}$ is due to the existence of N large ($\ell \gg \text{TeV}^{-1}$) extra dimensions into which the gravitational flux can spread out. At the distances larger than the typical size of these extra dimensions the gravity goes to its standard Einstein form, and the usual Newtonian low can be recovered via the relation $M_{Pl} = M^{N+2}\ell^N$ [5] between Plank scale and scale M . It means that, such kind of quantum gravity becomes strong at the energies M , where presumably all the interactions must

unify, without any hierarchy problem. The phenomenological implications of large extra dimensions is concentrated on the effects of real and virtual graviton emission. The basic assumption is, that gravitons can propagate in extra dimensions [5]. The quantum states of such gravitons are characterized by quantized momentum in the large extra dimensions. The only known framework that allows a selfconsistent description of quantum gravity is string theory. As an essential part of the structure of string theory [13] is that the gravitons and the particles of standard model must have an extended structure. This means that, there will be additional modifications of standard model amplitudes due to string excitations which can compete with or even overwhelm the modifications due to graviton exchange [6,7]. An important effects of simple model of string theory with large extra dimensions [7] come from the exchange of string Regge (SR) excitations of standard particles. In standard model scattering processes, contact interactions due to SR exchange produce their own characteristic effects in differential cross section, and these effects typically dominate the effects due to Kaluza – Klein (KK) exchange [5]. The SR excitation effects can be visible as contact interactions [6,7] well below the string scale M_S . The deviation from the standard model, we investigated, has been performed in the terms of Drell’s parameterization (5). Actually, this parameterization is applicable to any beyond standard model at short distances. Thus, from the comparison of string theory result [7] to the (5) the following identification can be deduced: $\Lambda_+ = \left(\frac{12}{\pi^2}\right)^{1/4} M_S$. Our result $\Lambda_+ > 415$ GeV corresponds to $M_S > 396$ GeV at 95% C.L. Using the connection between string scale and quantum gravity scale M [7] we find $M > 1188$ GeV.

REFERENCES

1. Berends, F. A., *Nucl. Phys.* **B186**, 22 (1981).
2. Eboli, O. J. P., Natale, A. A., and Novaes, S. F., *Phys. Lett.* **B271**, 274 (1991).
3. A. Litke, Harvard Univ., *Ph.D Thesis*, unpublished (1970).
4. Dymnikova, I., Ulbricht, J., and Zhao, J., this volume.
5. Arkani–Hamed, N., Dimopoulos, S., and Dvali, G., *Phys. Lett.* **B429**, 263 (1998); Antoniadis, I., Arkani–Hamed, N., Dimopoulos, S., and Dvali, G., *Phys. Lett.* **436**, 257 (1998).
6. Accomando, E., Antoniadis, I., and Benakli, K., *Nucl. Phys.*, **579B**, 3 (2000).
7. Cullen, S., Perelstein, M., and Peskin, M. E., *Phys. Rev.* **D62**, 055012 (2000).
8. L3 Collaboration, Acciarri, M., et al, *Phys. Lett.* **B475**, 198 (2000).
9. DELPHI Collaboration, Abreu, P., et al, *Phys. Lett.* submitted; ALEPH Collaboration, Barate, R., et al, *Phys. Lett.* **B429**, 201 (1998); OPAL Collaboration, Abbiendi, K., et al, *Phys. Lett.* **B465**, 303 (1999).
10. L3 Collaboration, Adeua, B., et al, *Nucl. Inst. Meth.* **A289**, 35 (1990).
11. L3 Collaboration, Adrian, O., et al, *Phys. Rep.* **236**, 1 (1990).
12. Harris, I., and Brown, L. M., *Phys. Rev.* **105**, 1656 (1957).
13. Polchinsky, J., “*String Theory*”, Camrige University Press (1998).